Avoid Frequency Extrapolation Errors

Relying on frequency extrapolations of known measured data can lead to erroneous simulations of S-parameter responses in commercial simulators, for active and passive models.

THOMAS WELLER, PH.D., LAWRENCE DUNLEAVY, PH.D., AND WILLIAM CLAUSEN

Modelithics, Inc., 13101 Telecom Dr., Suite 105, Temple Terrace, FL 33637-0914; (813) TO-MODEL, e-mail: ldunleavy@modelithics.com, Internet: www.modelithics.com.

Extrapolation of unknown frequency data for computer-aided-engineering (CAE) models can translate to misleading results. Measured scattering (S)-parameter data sets for passive components and transistors are fine for linear simulations that do not go outside the frequency limits of the measurement. But nonlinear harmonic-balance simulations, by their nature, require simulations at 5 to 10 harmonics of the desired operating frequency. Commercial simulators can extrapolate these higher harmonic information based on known lower-frequency measured data for active and passive devices, but these extrapolations often lead to nonphysical and inaccurate simulation results. Examples for this effect will be presented for a surface-mount capacitor and a high-electron-mobility transistor (HEMT).

Broadband frequency sweeps are often necessary when designing RF/microwave circuitry using CAE tools. For example, when performing nonlinear circuit simulations such as harmonic-balance simulations, it is common to include 5 to 10 harmonics of the fundamental design frequency. Components contained within a circuit schematic are also required to be valid at DC if these components are part of a DC path (e.g., bias paths for transistors). An ideal situation should include circuit models for all of the circuit components that are at best accurate, and at the least, well-behaved from DC through five or ten times the anticipated frequency of interest.

Properly performed S-parameter measurements can be used in combination with physically motivated equivalent-circuit topologies to produce valid broadband circuit models. In some cases, the S-parameter measurements themselves are a useful substitute for a physical model. The use of these measure-

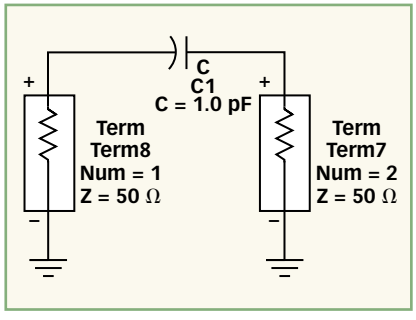

1. This schematic diagram shows an ideal 1-pF capacitor.

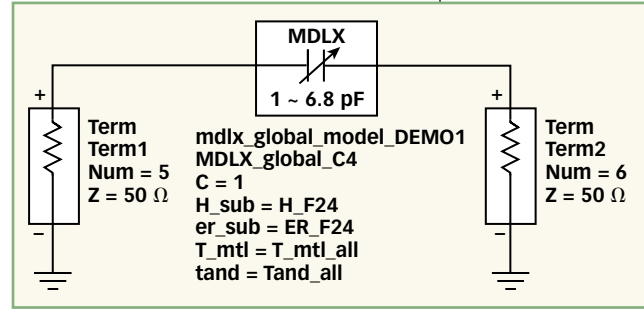

2. This substrate-scalable global capacitor equivalent-circuit model has been set to 1 pF.

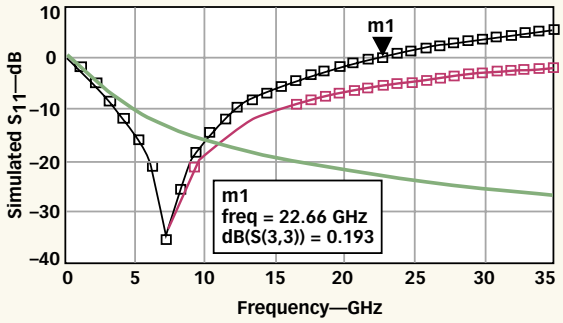

3. These simulated S_{11} responses for an ideal capacitor (thick black line), equivalent circuit model (magenta circles), and as extrapolated from a data set truncated at 6 GHz (blue squares).

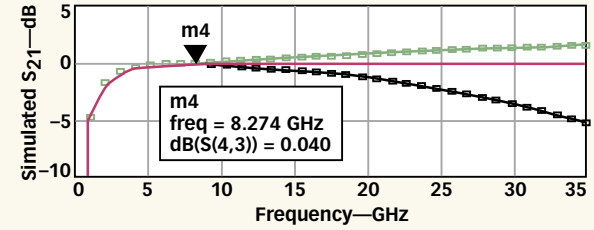

4. These simulated S_{21} results are shown for an ideal capacitor (thick black line), equivalent-circuit model (magenta circles), and as extrapolated from a data set truncated at 6 GHz (blue squares).

ments avoids errors associated with model extraction and/or curve/data fitting. In a similar way, electromagnetic (EM) simulation can be used to generate S-parameter data sets for arbitrary two- and three-dimensional (2D and 3D) passive structures.

Some simple examples may be useful in demonstrating the potential pitfalls that can occur during broadband and/or DC simulations. The particular situation addressed is that when S-parameter-based "data-set models" are used, in comparison to equivalent circuit models, in these simulations.

The first modeling example features the effects of performing passive simulations using different sets of data and a typical high-frequency component model, a 1-pF capacitor. Simulations will be compared for:

1. An ideal 1-pF capacitor in a series two-port configuration **(Fig. 1)**.
2. A measured S-parameter data set for a 1-pF capacitor, with data from 0.05 to 6.00 GHz. The original data set was extended through 10 GHz but truncated for the purpose of this example.
3. A substrate-scalable equivalent-circuit model for a 1-pF capacitor extracted from the measured (through 10 GHz) S-parameter data set prior to truncation **(Fig. 2)**.

The simulated S_{11} responses for the three modeling approaches are shown in **Fig. 3**. The frequency is swept from 0.05 to 35 GHz, which would provide coverage through the sixth or seventh harmonic of a 5-GHz wireless-local-area-network (WLAN) design. In this example, the response

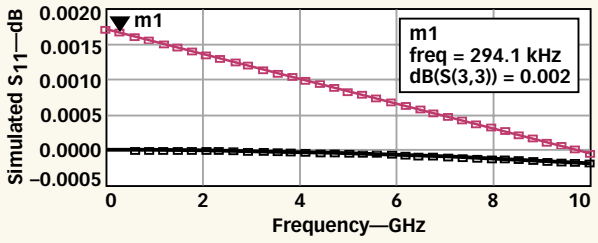

5. These simulated S_{11} results are shown for an ideal capacitor (no marker), equivalent-circuit model (magenta circles), and as extrapolated from a data set truncated at 6 GHz (blue squares).

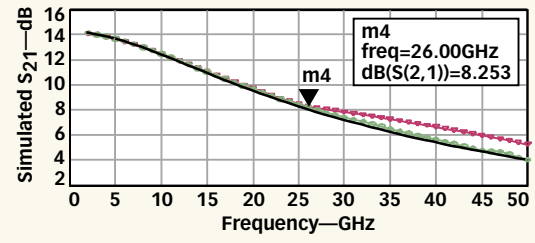

6. These plots compare S_{21} simulations for frequency extrapolations from the 26-GHz data set (red triangles) and the equivalent-circuit model (bold black line) to the 50-GHz data (blue circles).

of the ideal capacitor is inaccurate after approximately 3 GHz, while the equivalent-circuit model tracks the measurement data through 7 GHz. Most significantly, the extrapolation of the measured data set beyond its upper limit (6 GHz) leads to a *nonphysical* result of $S_{11} > 0$ dB past 22 GHz. The response of the equivalent-circuit model, on the other hand, has a well-behaved monotonic increase toward (but not exceeding) 0 dB.

The simulated S_{21} responses for the same 0.05 to 35 GHz sweep are shown in **Fig. 4.** In this case the extrapolated S_{21} from the measurement data set goes above 0 dB (indicating gain for a passive) at 8 GHz, which is only slightly beyond the upper limit of the S-parameter file.

The low-frequency S_{11} responses of the schematics are shown in **Fig. 5.** As would be expected, the ideal capacitor response is indistinguishable from the equivalent-circuit model prediction since any parasitic effects are negligible. However, the extrapolation of the measurement data set once again leads to a nonphysical result of $S_{11} > 0$. This result can lead to convergence errors during harmonic-balance simulations (e.g., analysis of microwave mixers and frequency converters). Similar problems arise in inductor, filter, and passive matching network extrapolations.

To understand the active-device simulation issue, HEMT S-parameters generated within a commercial CAE simulator were compared for:

1) A measured data set whose upper frequency limit is 26 GHz.
2) A measured data set whose upper frequency range is 50 GHz.
3) An accurate broadband equivalent-circuit model for the HEMT.

Figure 6 offers a comparison of S_{21}

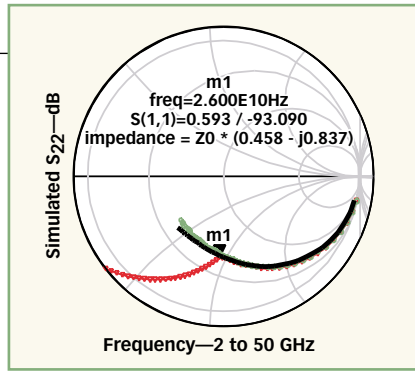

7. These plots show a HEMT transistor S_{22} comparison of frequency extrapolation from 26-GHz data set (red triangles) and circuit model (bold black line) to 50-GHz data (blue circles).

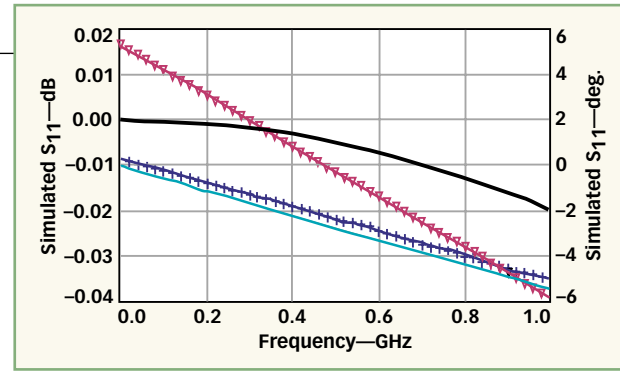

8. These plots show low-frequency extrapolation of HEMT S_{11} data from a 2-to-26-GHz data set (red triangles = magnitude, blue circles = phase) compared to equivalent-circuit simulations (bold black line = magnitude, green line = phase).

forward-transmission swept-frequency simulation responses from 2 to 50 GHz for the two measurement data sets compared to the equivalent-circuit model for the HEMT. The equivalent-circuit model matches closely with the 50-GHz measured data set. As expected, the S_{21} simulations based on the 26-GHz data set agree well with the simulations for the equivalent-circuit model and the 50-GHz data through 26 GHz, but deviate beyond 26 GHz, clearly showing the errors resulting from the frequency extrapolation. Significant problems are also apparent in the S_{22} comparison shown in **Fig. 7**, with the extrapolated data set departing significantly from the broadband measurement and the model above its frequency limit.

Since low-frequency data can be essential to the biasing of a HEMT device, low-frequency extrapolations were made for S_{11} **(Fig. 8)** simulations of the HEMT. The basic 2-to-26-GHz data set was extrapolated to the DC-to-1-GHz range and compared to the results for the equivalent-circuit model. Problems with the data extrapolation are evident in the S_{11} data near DC. For the extrapolations, the magnitude of S_{11} rises above 0 dB, indicating an instability not shown in the model simulations. The phase of S_{22} (not shown) also exhibits a nonphysical result, with positive reactance below 200 MHz. MRF

EDITOR'S NOTE

Thomas Weller, Ph.D. and Lawrence Dunleavy, Ph.D. are also affiliated with the Dept. of Electrical Engineering at the University of South Florida in Tampa, FL.

Fast and Efficient Algorithms in Computational Electromagnetics

WENG CHO CHEW, JIAN-MING JIN, ERIC MICHIELSSEN, AND JIMING SONG

Fast and Efficient Algorithms in Computational Electromagnetics documents recent advances in computational EMs in the manner of a monograph. For those who intend to perform research in this area, this book will be an excellent starting point, as it focuses on linear problems associated with Maxwell's equations.

Chapter 1 introduces EM analysis and explains how the field has evolved into computational EMs in the last few decades. It also introduces, in a very simplified manner, the recent fast algorithms developed to solve Maxwell's equations.

FMM and MLFMA in 2D are introduced in Chapter 2. Interpolation, truncation, and integration efforts are discussed. An attempt is also made to relate FMM to group theory, and to the inherent symmetry of space. Chapter 3 describes the 3D version of FMM and MLFMA and demonstrates the application of the fast algorithm to real-world problems.

Distributed-memory parallelization of MLFMA, encapsulated in a code known as ScaleME is reviewed in Chapter 4. The parallelization of MLFMA on a distributed memory machine is not an easy task, because different parts of the computation may reside on different processors.

Low-frequency solution of Maxwell's equations using fast algorithms is presented in Chapter 5. This chapter describes the treatment needed for FMM and MLFMA to prevent their catastrophic breakdown at low frequencies. It also describes a method to apply the LF-MLFMA based on RWG, wire, and wire-surface bases while the intrinsic expansion bases are still the loop-tree-star bases.

Different error issues involved when solving surface integral equations related to Maxwell's theory are reviewed in Chapter 6. Discretization error due to the use of basis functions and integration error by replacing integrals with summation are included. The chapter also discusses deconditioning due to the near-resonance problem and the low-frequency breakdown problem.

Chapter 7 deals with a recent topic of intense interest in differential equation solvers—the theory of PML. The concept of complex coordinate stretching is discussed. PML is generalized to curvilinear coordinates, as well as to complex media. In this chapter, stability issues related to PML are studied and a unified analysis of various PML formulations using differential forms is included. Chapter 8 addresses the issue of efficiently solving the forward and inverse problems for buried objects using FFT-based methods. The detection of buried objects usually involves loop antennas, and the forward problem involving the solution of loop antennas over a buried object is discussed in detail. Moreover, recent advances in different inversion algorithms are also described.

Solving the penetrable problem at very low frequencies is the focus of Chapter 9. The low-frequency problem encountered in Chapter 5 for metallic objects also occurs for dielectric and lossy material objects. This chapter describes a way to solve this problem so that the solution of integral equations remains stable from zero frequency to microwave frequencies.

Chapter 10 describes an algorithm to solve 3D waveguide structures using numerical-mode matching, but using the finite difference method. The spectral Lanczos decomposition method is used to find the modes. An algorithm with $O(N)$ memory complexity and $O(^{NI-5})$ computational complexity is achieved. Chapter 11 addresses the problem of solving the volume integral equation concurrently with the surface integral equation. This is particularly important when dealing with structures having metals as well as dielectric materials.

Chapter 12 deals with solving axially symmetric, BOR geometry using FEM. This reduces a 3D problem to 2D, greatly enhancing the efficiency of the solution. Material-coated and metallic objects are considered. Hybridization in computational EMs is the topic of Chapter 13. Hybridization between FEM and ABC is discussed along with BIE, MLFMA, AABC, and SBR. Hybridization between MOM and SBR is also considered. AABC is a promising method of hybridizing FEM with fast solvers for the future.

Chapter 14 presents different higher-order methods for computational EMs, surface integral equations, and FEM. In addition, the efficient coupling of higher-order methods to fast solvers such as MLFMA is discussed. Chapter 15 discusses AVVE for broadband calculation in EMs. Illustrations of this acceleration technique for broadband calculation are provided for metallic antennas, wire antennas, dielectric scatterers, and microstrip antennas.

Microstrip structure analysis on top of a layered medium is detailed in Chapter 16. The derivation of the layered-medium Green's function together with its numerical approximation by the complex images is discussed. The use of the fast-frequency sweep method, adaptive integral method, and MLFMA to accelerate solution speed is studied. A higher-order method to improve solution accuracy is also demonstrated.

Chapter 17 reviews SDFMM to accelerate the solution speed of quasi-planar structures. For this class of structures, this method reduces the computational and memory complexity of MLFMA from $O(N \log N)$ to $O(N)$. Applications to scattering from random rough surfaces, quantum-well gratings, and microstrip antennas are demonstrated with this analysis method.

Chapter 18 elaborates on the PWTD algorithm, which is an ingenious way of arriving at the time-domain equivalent of FMM and MLFMA. The integral equation is solved using the MOT method. Stability and accuracy issues are carefully analyzed in this chapter. The two-level and multilevel algorithms are presented and demonstrated with examples.

Chapter 19 further develops PWTD for large-scale and real-world applications. The use of PWTD with MFIE, EFIE, and CFIE is illustrated. (2001, 931 pp., hardcover, ISBN: 1-58503-152-0, $129.00.) **Artech House, 685 Canton St., Norwood, MA 02062; (781) 769-9750, FAX: (781) 769-6334, Internet: www.artech-house.com.**